Kinetics of Heterogeneous Reaction of Sulfur Dioxide on Authentic Mineral Dust: Effects of Relative Humidity and Hydrogen Peroxide

Liubin Huang, Yue Zhao,[†] Huan Li, Zhongming Chen[*]

State Key Laboratory of Environmental Simulation and Pollution Control, College of Environmental Sciences and Engineering, Peking University, Beijing 100871, China

[*] Corresponding Author: zmchen@pku.edu.cn

[†] Present Address: Department of Chemistry, University of California, Irvine, California 92697, USA

15 pages, 3 Tables, 8 Figures

1. The preparation of dust-deposited filters

Mineral dust particles were resuspended using a custom-designed resuspension apparatus and subsequently collected on the filters. The schematic diagram of the resuspension apparatus is shown in Figure S1. The apparatus consists of a glass inlet, a diffusion tube (inner diameter 45 mm), a stainless filter holder and a pump. The mineral dust particles were placed into the "T" shape glass tube. The inlets of the glass tube were closed and the system was pumped. After a few second when a negative pressure was formed in the system, the inlets of the glass tube were reopened, and the mineral dust particles were carried by a flow (16.7 standard L min^{-1}) of air, into the diffusion tube, where the particles were effectively resuspended, and subsequently collected onto the filter.

2. Porosity measurements for AMD, TDD and ATD particles

We have employed different methods to identify the porosity of mineral dust. First, we used field emission scan electron microscopy (FESEM, Zeiss, Merlin Compact) to

directly observe the morphology of mineral dust (Figure S5), and found that the mineral dust really has some pores (see the mark in Figure S5). Second, pore size distributions of mineral dust were measured by Pore size distribution analyzer (Micrometritics, ASAP2010), the isotherm plots of AMD, TDD and ATD particles are shown in the Figure S6. It is shown that the desorption curve is not coincide with the adsorption curve due to the capillary condensation effect, leading to the occurrence of a hysteresis loop.[1,2] The hysteresis loop is closely associated with the shape and size of the pores. The existence of the hysteresis loop indicates that mineral dust is porous and most of pores are mesoporous (2–50 nm). Furthermore, according to the shape of hysteresis loop (i.e., H3 hysteresis loop, for which the adsorption curve does not flatten at higher relative pressures),[1,2] we can inferred that these pores are slits, which has been frequently found in the clays, e.g., kaolinite.[2] Figure S7 shows the pore size distributions of AMD, TDD and ATD particles. It can be seen that the smaller pores have a much larger contribution to the total pore volume, compared to the larger pores. This further establishes that the mineral dust is porous. Figure S8 shows the BJH adsorption accumulative pores surface area of particles, which represents the total internal surface area contributed by all of the pores larger than a given diameter. For instance, the BJH adsorption accumulative surface area of pores (1.7 nm) for AMD, TDD and ATD particles were measured to be 6.8, 5.7 and 10.4 $m^2\ g^{-1}$, respectively. The BJH surface area and the BET surface area, measured by the same instrument, represent the internal surface area of particles in a way and the total surface area of particles, respectively. But it is not reasonable to equate the difference between BJH and BET surface areas to the external surface area of the particles, since the calculation methods for estimating the BJH and BET surface areas are significantly different. For the same reason, the BJH surface area of AMD and TDD particles are found to be slightly higher than their BET surface area (i.e., 6.1 and 4.0 $m^2\ g^{-1}$ for AMD and TDD particles, respectively). Nevertheless, these results provide semi-quantitative information on the surface area of pores, which likely accounts for a significant portion of the total surface area of mineral dust particles.

3. The diffusion mode of SO_2 in the pore of the particles

The modes of gas-phase diffusion in the pore of the particles include Knudsen diffusion, molecular diffusion, and configuration diffusion.[2,3,4] In our study, the mean free path (λ) of SO_2 was estimated to be ~1.16×10^{-7} m at 298K and atmospheric pressure, and the average pore diameter (d) of AMD, ATD and TDD particles was measured as 13, 5.5 and 16 nm, respectively. The ratios of λ to d are larger than 10 for all three mineral dust particles. Therefore, the gas-diffusion in the pore of the particles follows Knudsen diffusion.

4. The expression for the surface reaction rate constant

The loss rate of gas species, C per unit volume can be express as eq 1[5]

$$-\frac{d[C]}{dt} = \frac{\gamma_c \omega A[C]}{4V} \quad (1)$$

where [C] is the gas concentration of SO_2; γ_c is the corrected uptake coefficient; ω is the mean molecular velocity, m s^{-1}. A/V is the surface area density of particles, m^{-1}.

In term of eq (1), the first-order loss rate constant k can be given by eq 2[5,6]

$$k = \frac{\gamma_c \omega A}{4V} \quad (2)$$

And the k_t, defined as the surface reaction rate constant normalized to the particle surface area density, m s^{-1}, can be derived from eq 3

$$k_t = \frac{\gamma_c \omega}{4} \quad (3)$$

5. The surface area density of mineral dust in summer and winter in Beijing

It was reported that in Beijing, the average surface area density of aerosols (0–10 μm) is 1.4×10^{-5} cm^2 $cm^{-3}$and the corresponding PM_{10} concentration is 135 μg m^{-3}.[7] Zhang et al[8] found that the average $PM_{2.5}$ concentration is 138 μg m^{-3} in summer and 139 μg m^{-3} in winter, and the proportion of mineral dust in $PM_{2.5}$ is 8.2% in summer and 28.9% in winter. According to the ratio of $PM_{2.5}$ to PM_{10} in summer (49%) and winter (66%),[9] the PM_{10} concentration is estimated as 282 μg m^{-3} in summer and 211 μg m^{-3} in winter. Assuming that in Beijing, the size distribution of mineral dust is similar to PM_{10} and the proportion of mineral dust in PM_{10} is similar to that in $PM_{2.5}$, we

estimate the surface area density of mineral dust to be 2.4×10^{-6} cm^2 cm^{-3} in summer and 6.3×10^{-6} cm^2 cm^{-3} in winter.

References

(1). Ruthven, D. M. *Principles of Adsorption and Adsorption Processes;* John Wiley & Sons, **1984**.

(2) Suzuki, M. *Adsorption Engineering;* Kodansha: Elsevier, **1990**.

(3) Aris, R. *The Mathematical Theory of Diffusion and Reaction in Permeable Catalysts;* Clarendon: Oxford, **1975**.

(4) Satterfield, C. N. *Mars Transfer in Heterogeneous Catalysis;* MIT Press: Cambridge, MA, **1970**.

(5) Molina, M. J.; Molina, L. T. Environmental chemistry (gas and gas-solid interactions): The role of physical chemistry. *J. Phys. Chem.* **1996**, *100*, 12888–12896.

(6) Ravishankara, A. R. Heterogeneous and multiphase chemistry in the troposphere. *Science* **1997**, *276*, 1058–1065.

(7) Wehner, B.; Birmili, W.; Ditas, F.; Wu, Z.; Hu, M.; Liu, X.; Mao, J.; Sugimoto, N.; Wiedensohler, A. Relationships between submicrometer particulate air pollution and air mass history in Beijing, China, 2004–2006. *Atmos. Chem. Phys.* **2008**, *8*, 6155–6168.

(8) Zhang, R.; Jing, J.; Tao, J.; Hsu, S. C.; Wang, G.; Cao, J.; Lee, C. S. L.; Zhu, L.; Chen, Z.; Zhao, Y.; Shen, Z. Chemical characterization and source apportionment of $PM_{2.5}$ in Beijing: seasonal perspective. *Atmos. Chem. Phys.* **2013**, *13*, 7053–7074.

(9) Yang, F. M.; He, K. B.; Ma, Y. L.; Zhang, Q.; Yu, X. C. Variation characteristics of $PM_{2.5}$ concentration and its relationship with PM_{10} and TSP in Beijing. *China Environ. Sci*. **2002**, *22*, 506–510.

Table S1. Typical compositions of AMD, TDD and ATD particles.

Composition	Weight percentage (%)		
	AMD	**TDD**	**ATD**
SiO_2	51.5±0.25	55.9±0.25	68.8±0.23
Al_2O_3	15.5±0.18	13.7±0.17	13.3±0.17
CaO	7.25±0.13	8.55±0.14	3.02±0.09
Fe_2O_3	4.54±0.10	3.88±0.10	2.60±0.08
MgO	3.56±0.09	3.36±0.09	1.71±0.06
Na_2O	2.55±0.08	2.21±0.07	2.28±0.07
K_2O	2.39±0.08	2.08±0.07	2.56±0.08
TiO_2	0.68±0.03	0.76±0.04	0.43±0.02

Table S2. Parameters for correcting the uptake coefficient of SO_2 on AMD, TDD, and ATD particles under dry condition.

Parameters	**AMD**	**TDD**	**ATD**
S_g **(m^2 g^{-1})**	6.1	4.0	16.5
R_p **(μm)**	10.8	11.1	2.4
S_e **(m^2 g^{-1})**	0.30	0.23	0.67
V_g **(cm^3 g^{-1})**	0.020	0.016	0.023
τ	2	2	2
ρ_p **(g cm^{-3})**	2.65	2.65	2.65
γ_{BET} **(×10^{-5})**	3.15±0.33	3.81±0.25	1.31±0.05
η	0.28	0.11	0.095
γ_c**(×10^{-4})**	2.14±0.23	2.29±0.15	0.35±0.01
γ_c / γ_{BET}	7.14	6.03	2.67

Note: S_g, the BET specific surface area; R_p, the average radius of the particles; S_e, the external specific surface area of particles, can be obtained from the size distribution of particles (see Figure S2); V_g, the pore volume of the particles; τ, the tortuosity factor; ρ_p, the bulk density of mineral dust; η, the effectiveness factor; $\gamma_{BET,}$ the uptake coefficient calculated using BET surface area as the effective surface area of the particles; γ_c, the corrected uptake coefficient.

Table S3. γ_{BET} and γ_{ext} of SO_2 on AMD, TDD, and ATD particles in the absence and presence of H_2O_2 at different RHs.

RH (%)	AMD				TDD				ATD			
	γ_{BET} ($\times10^{-5}$)		γ_{ext} ($\times10^{-4}$)		γ_{BET} ($\times10^{-5}$)		γ_{ext} ($\times10^{-4}$)		γ_{BET} ($\times10^{-5}$)		γ_{ext} ($\times10^{-4}$)	
	N[a]	Y	N	Y	N	Y	N	Y	N	Y	N	Y
0	3.15±0.33	4.52±0.53	5.82±0.61	8.36±0.98	3.81±0.25	5.35±0.37	6.62±0.43	9.30±0.64	1.31±0.05	1.74±0.15	3.23±0.12	4.29±0.37
15	2.72±0.26	3.46±0.26	5.03±0.48	6.40±0.48	3.62±0.53	5.09±0.55	6.29±0.92	8.85±0.96	1.43±0.03	2.04±0.23	3.52±0.07	5.02±0.57
30	2.85±0.35	5.09±0.32	5.27±0.65	9.40±0.59	4.19±0.56	5.60±0.50	7.29±0.97	9.74±0.87	1.58±0.4	2.67±0.45	3.89±0.99	6.58±1.11
45	2.54±0.35	5.06±0.58	4.70±0.65	9.35±1.07	4.48±0.42	6.08±0.23	7.79±0.73	10.5±0.40	1.92±0.39	2.24±0.21	4.73±0.96	5.52±0.52
60	2.35±0.28	6.45±0.62	4.34±0.52	11.9±1.14	5.37±0.25	6.56±0.56	9.34±0.43	11.4±0.97	2.11±0.30	2.73±0.36	5.20±0.74	6.72±0.89
75	2.15±0.40	6.06±0.50	3.97±0.74	11.2±0.93	5.28±0.51	7.51±0.63	9.18±0.89	13.1±1.09	2.46±0.32	3.11±0.29	6.01±0.79	7.66±0.71
90	1.85±0.36	5.87±0.48	3.42±0.67	10.9±0.89	5.52±0.63	7.83±0.55	9.60±1.09	13.6±0.96	2.76±0.25	4.43±0.52	6.79±0.62	10.9±1.28

[a]N, without H_2O_2; Y, with H_2O_2. γ_{BET} and γ_{ext} represent the uptake coefficients calculated using the BET surface area and external surface area of mineral dust particles, respectively.

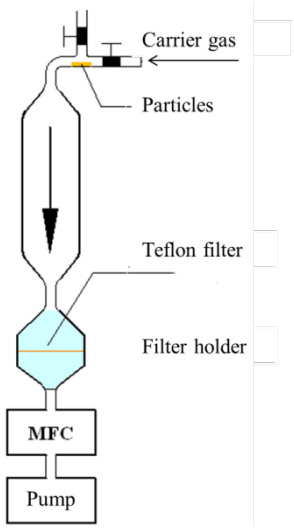

Figure S1. Schematic diagram of the resuspension apparatus. MFC, mass flow controller.

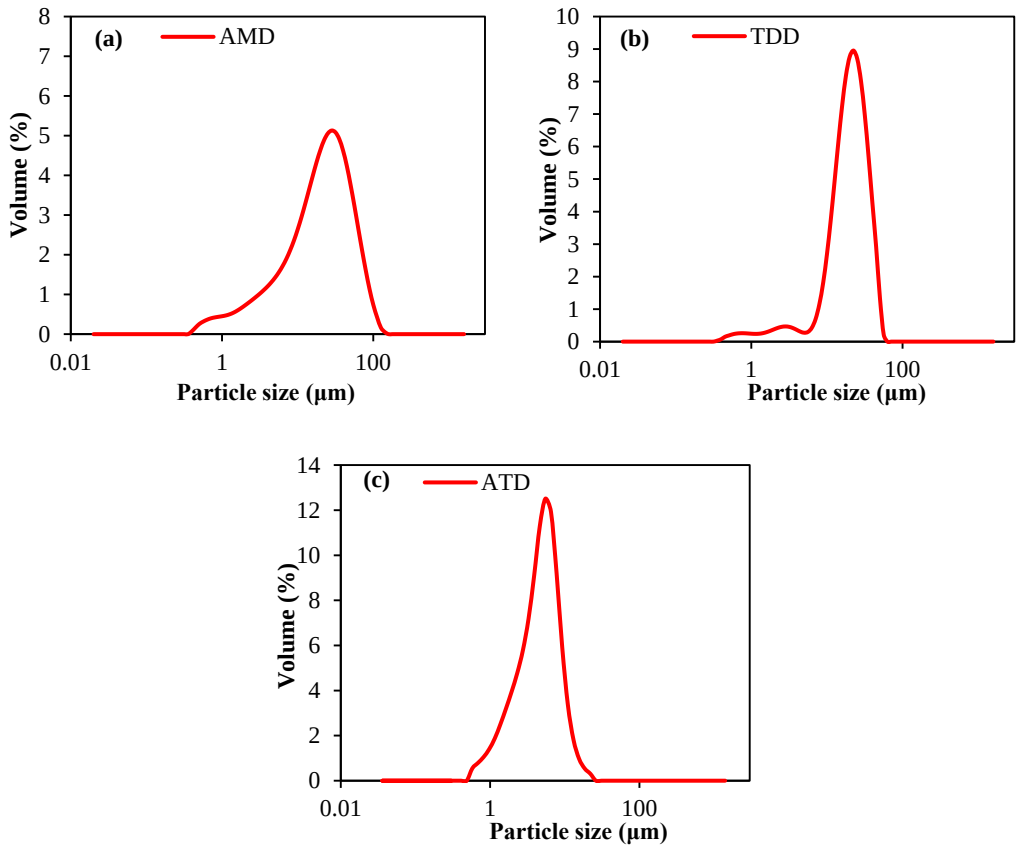

Figure S2. Particle size distribution of (a) AMD, (b) TDD, and (c) ATD particles

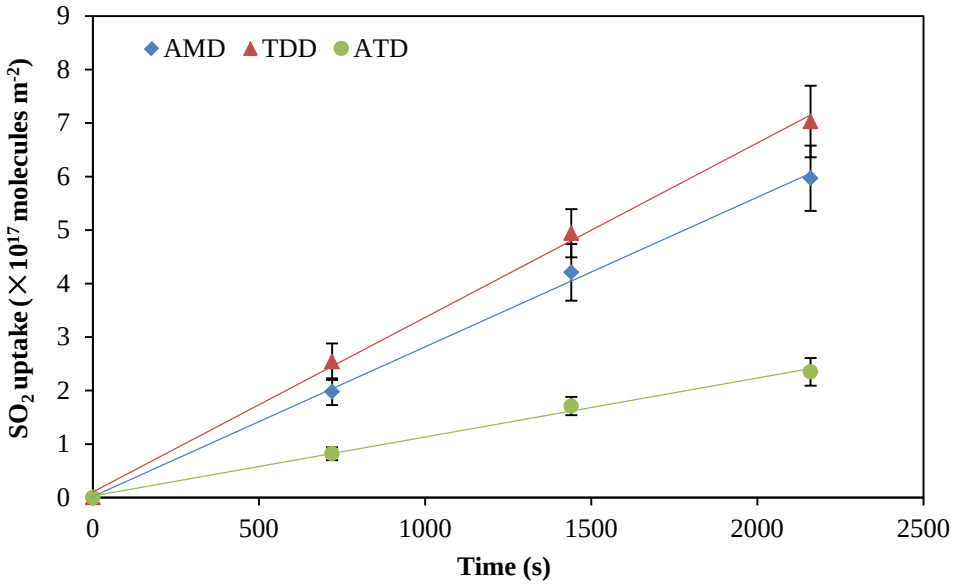

Figure S3. Amount of SO_2 taken up by AMD, TDD, and ATD particles in the absence of H_2O_2 as a function of reaction time under dry condition. The initial concentration of SO_2 is ~5 ppbv. Error bars represent 1σ.

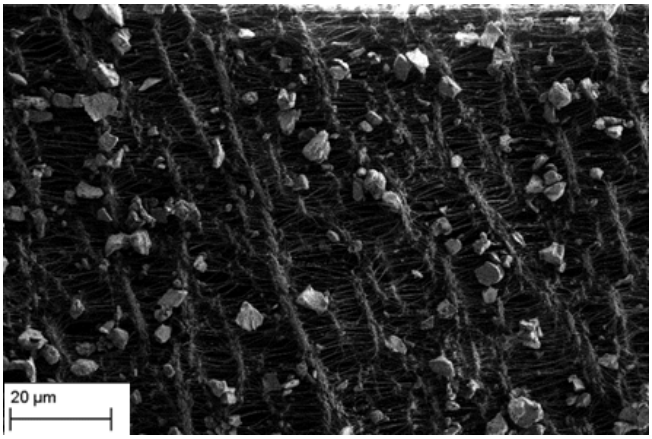

Figure S4. FESEM microphotograph of ATD particles on the PTFE filter. The particle mass collected on the filter is 0.86 mg.

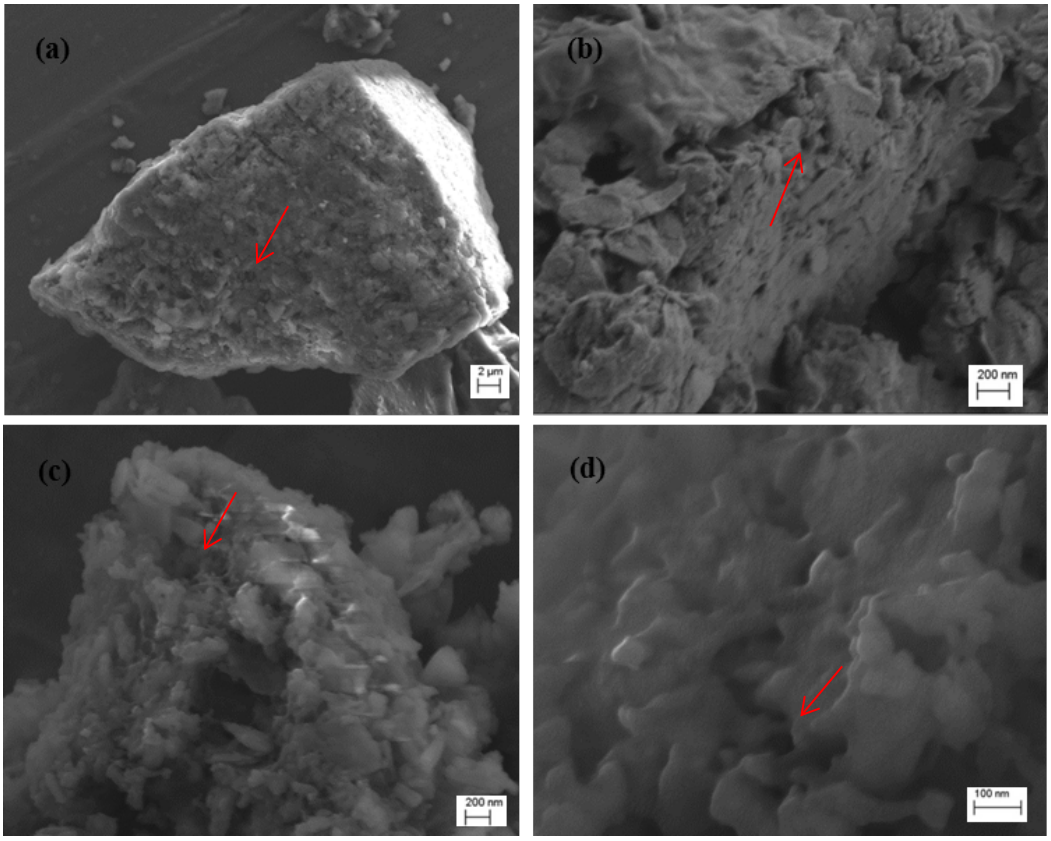

Figure S5. FESEM microphotographs of (a) AMD, (b), (c) TDD, and (d) ATD particles.

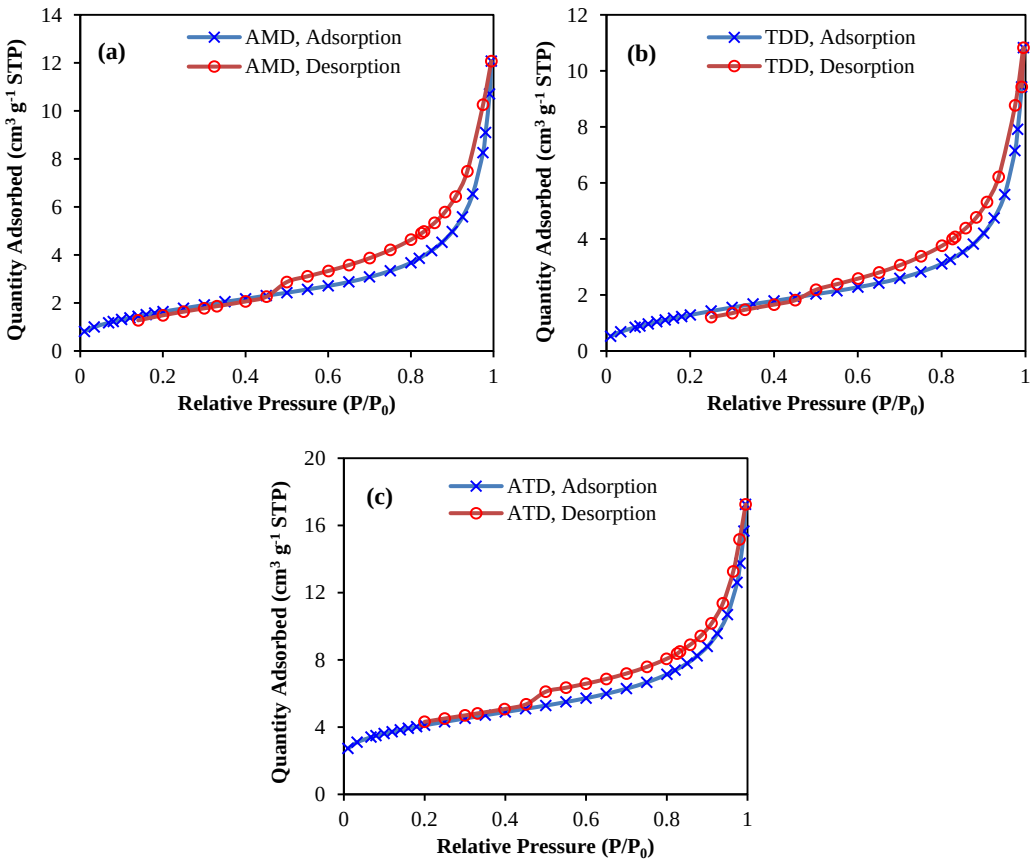

Figure S6. Isotherm plot of (a) AMD, (b) TDD, and (c) ATD particles.

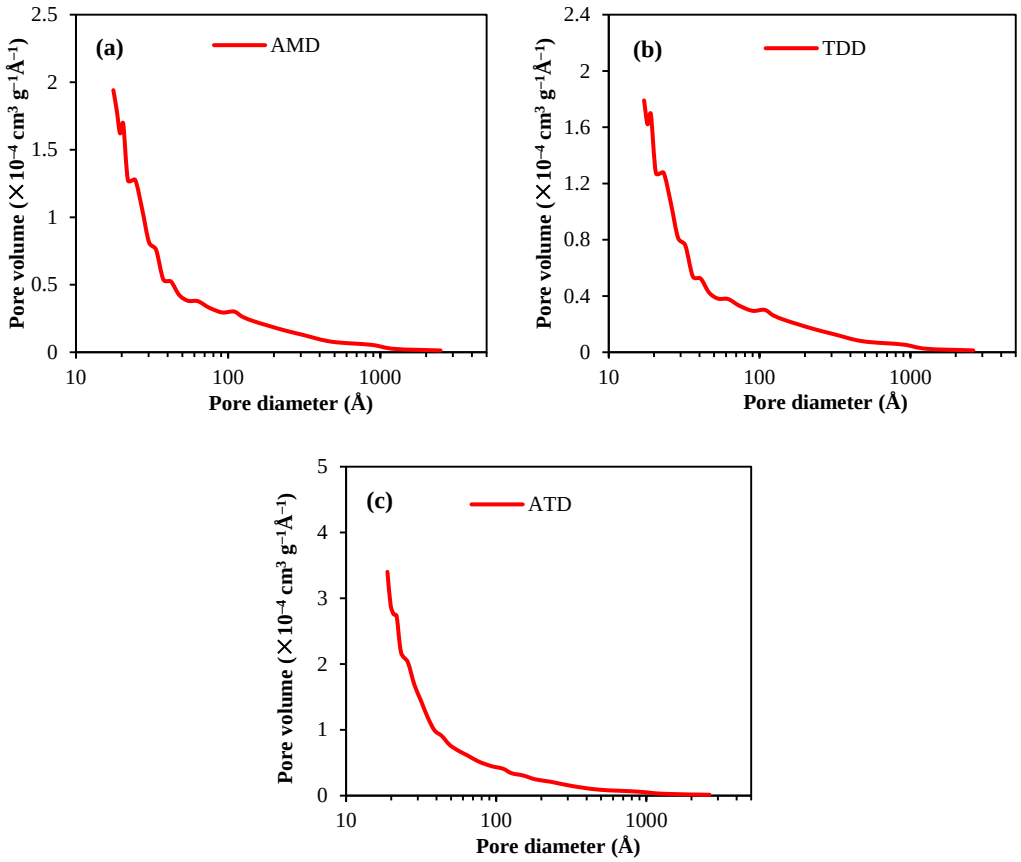

Figure S7. BJH (Barrett-Joyner-Halenda) adsorption *dV/dD* of (a) AMD, (b) TDD and (c) ATD particles. *V*, pore volume; *D*, pore diameter.

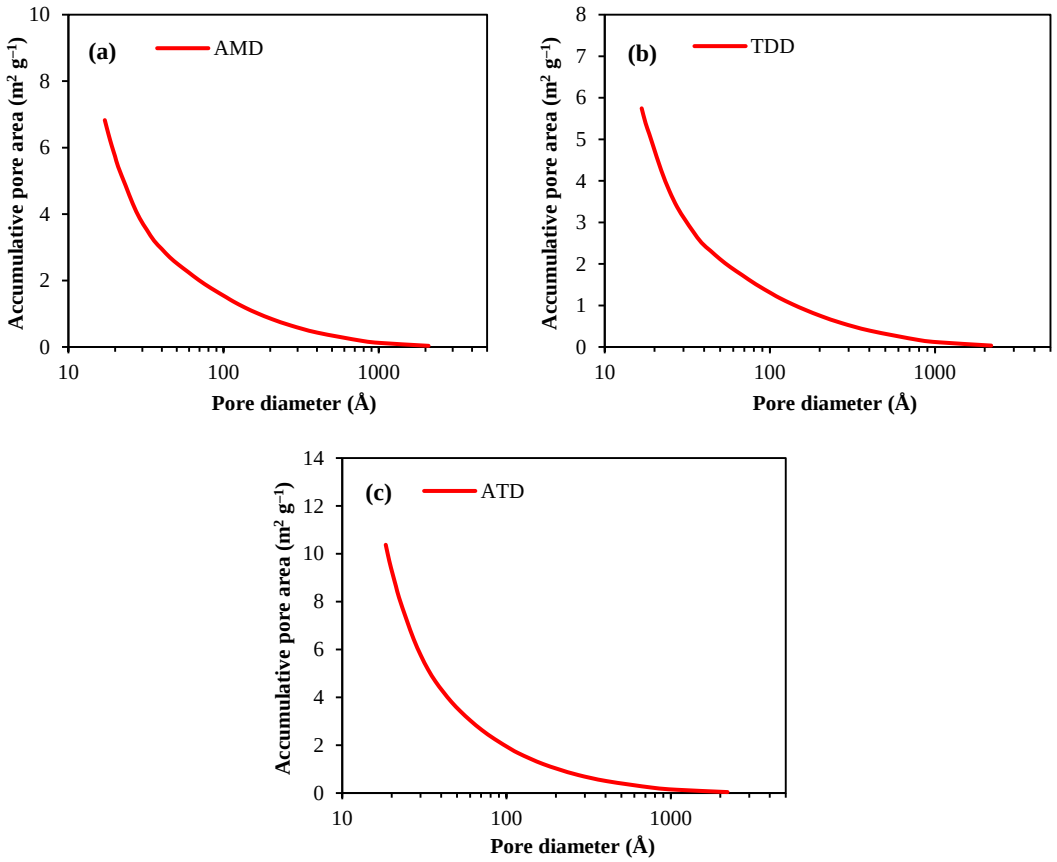

Figure S8. BJH adsorption accumulative pores surface area of (a) AMD, (b) TDD, and (c) ATD particles.